AFRL-RX-WP-TM-2014-X116

UNDERSTANDING THERMAL TRANSPORT IN GRADED, LAYERED AND HYBRID MATERIALS

Jonathan E. Spowart
AFRL/RXCCM

Vikas Sinha
UES, Inc.

APRIL 2014
Final Report

STINFO COPY

AIR FORCE RESEARCH LABORATORY
MATERIALS AND MANUFACTURING DIRECTORATE
WRIGHT-PATTERSON AIR FORCE BASE, OH 45433-7750
AIR FORCE MATERIEL COMMAND
UNITED STATES AIR FORCE

NOTICE AND SIGNATURE PAGE

//Signature//   //Signature//
_____   _____
JONATHAN E. SPOWART, Project Engineer   SEAN C. COGHLAN, Chief
Composite Materials & Processing Section Composite Materials & Processing Section
Composites Branch   Composites Branch
Structural Materials Division   Structural Materials Division

//Signature//
_____
ROBERT T. MARSHALL, Deputy Chief
Structural Materials Division
Materials and Manufacturing Directorate

REPORT DOCUMENTATION PAGE

Form Approved
OMB No. 0704-0188

1. REPORT DATE (DD-MM-YY)	2. REPORT TYPE	3. DATES COVERED (From - To)
April 2014	Final	28 September 2011 – 31 March 2014

4. TITLE AND SUBTITLE
UNDERSTANDING THERMAL TRANSPORT IN GRADED, LAYERED AND HYBRID MATERIALS

5a. CONTRACT NUMBER
In-house

5b. GRANT NUMBER

5c. PROGRAM ELEMENT NUMBER
62102F

6. AUTHOR(S)
Jonathan E. Spowart (AFRL/RXCCM)

Vikas Sinha (UES, Inc.)

5d. PROJECT NUMBER
4347

5e. TASK NUMBER

5f. WORK UNIT NUMBER
X062

7. PERFORMING ORGANIZATION NAME(S) AND ADDRESS(ES)

AFRL/RXCCM
2941 Hobson Way
Wright-Patterson AFB, OH 45433

UES, Inc.
4401 Dayton-Xenia Road
Dayton, OH 45432

8. PERFORMING ORGANIZATION REPORT NUMBER

9. SPONSORING/MONITORING AGENCY NAME(S) AND ADDRESS(ES)
Air Force Research Laboratory
Materials and Manufacturing Directorate
Wright-Patterson Air Force Base, OH 45433-7750
Air Force Materiel Command
United States Air Force

10. SPONSORING/MONITORING AGENCY ACRONYM(S)
AFRL/RXCCM

11. SPONSORING/MONITORING AGENCY REPORT NUMBER(S)
AFRL-RX-WP-TM-2014-0116

12. DISTRIBUTION/AVAILABILITY STATEMENT
Approved for public release; distribution unlimited.

13. SUPPLEMENTARY NOTES
PA Case Number: 88ABW-2014-2880; Clearance Date: 11 June 2014. Report contains color.

14. ABSTRACT (Maximum 200 words)
The overall research goal is to gain a detailed understanding of thermal transport through multilayered interfaces between dissimilar materials, using a combination of time-domain spectroscopy, physical modeling and materials processing. Specific goals for the overall project include; (i) investigate the structure, thickness and morphology of the copper-diamond interface for various processing conditions; (ii) assess the effect of interfacial morphology on bulk thermal conductivity, using appropriate models; (iii) publish the results of experimental investigations into bulk thermal properties of copper-diamond composites with various interfacial chemistries, including metallic and carbide layers, and; (iv) mimic the observed interface structure on a TDTR specimen by manipulating the various deposition techniques available to us experimentally.

15. SUBJECT TERMS
copper-diamond interface, thermal conductivity, time-domain thermo-reflectance

16. SECURITY CLASSIFICATION OF:			17. LIMITATION OF ABSTRACT:	18. NUMBER OF PAGES	19a. NAME OF RESPONSIBLE PERSON (Monitor)
a. REPORT Unclassified	**b. ABSTRACT** Unclassified	**c. THIS PAGE** Unclassified	SAR	27	Jonathan E. Spowart
					19b. TELEPHONE NUMBER (Include Area Code) (937) 255-9277

TABLE OF CONTENTS

LIST OF FIGURES

1.0 TECHNICAL SUMMARY

Microstructural and chemical characterization of diamond particles with surface carbides, which were extracted from several different composites via acid dissolution of Cu, continued throughout the last 12 months of the effort. The previously-reported electron probe microanalysis (EPMA) based techniques were employed to estimate the interfacial carbide layer thickness for the different composites, including GMR analysis. In addition, unprocessed diamond particles were obtained from Fraunhofer, and these were acquired from the same source (Luoyang High-Tech Qiming Superhard Materials Co. Ltd, China) as the diamond used previously to fabricate the Fraunhofer-supplied CuCr-diamond composites. The nitrogen content of unprocessed diamond particles was determined using inert gas fusion technique (ASTM E 1019-08). The thermal conductivity of diamond was estimated from its nitrogen content, using the previously published data on variation of diamond thermal conductivity with a change in nitrogen content. This thermal conductivity of diamond was used to estimate the Cu/diamond interface thermal conductance (G $_{Cu/diamond}$) with the Hasselman and Johnson model, as well as per the Differential Effective Medium (DEM) scheme.

Thin metal films were deposited on the diamond substrates via magnetron sputtering, in order to investigate their effect on the measured thermal properties of the combined diamond-metal interface region. A direct current (DC) process was used for deposition of Cu top layer; whereas high power pulsed magnetron sputtering process was used for deposition of Ti-interface layer. This process differs from ordinary sputtering in that 1) the metal flux is composed primarily of ions rather than neutrals, and 2) the maximum kinetic energy of the incident ions is significantly larger (~10-15 eV) than in ordinary sputtering. The base pressure for magnetron sputtering apparatus was less than 5×10^{-9} Torr, and the pure metal (Ti and Cu) targets were sputtered in 10 mTorr of ultra-high purity Ar. The maximum temperature of the substrate surface during deposition was approximately 70 $^{\circ}$C as measured by a calibrated infrared pyrometer aimed at the sample surface.

In year 2 of the effort, TEM grids were acquired from Ted Pella, which consist of perforated membrane of Si-nitride with the hole diameter of 2.5 micrometers and a pitch of 4.5 micrometers. The perforated area is 0.45 mm X 0.45 mm, and is supported on a 3 mm diameter Si frame. These grids were used as masks to make discontinuous interface layer of Cr_3C_2 between Cu and diamond for TDTR experiments in an attempt to mimic the conditions of some of the actual Cu-diamond composites. In addition, a Cr_3C_2 target was acquired from Stanford Materials, which was used to deposit Cr_3C_2 interface layer via magnetron sputtering between Cu and diamond. These specimens were subsequently analyzed using TDTR to determine the Cu/diamond interface thermal conductance under the conditions of a Cr_3C_2 interface layer. In addition, deposition of Au through the Si-nitride holey grid on oxidized Si wafer was carried out using magnetron sputtering to replicate the pattern of holey grid on Si substrate. Deposition of Au through the SiN holey grid was successful. However, in this first attempt, the pattern of holey grid was not replicated on the oxidized Si wafer. No holes were observed in the coated (square) region of this sample. Due to this limited success, alternate approaches to replicate the pattern of holey grid were also attempted. In a second trial, Ti was deposited through the Si-nitride holey grid on Si wafer (non-oxidized) and the substrate was not rotated during sputter-deposition. Deposition of Ti through the holey grid was successful. The pattern of holey grid was replicated, at least to some extent, on the Si wafer. The thickness of Ti in the coated and uncoated/partially-coated regions was determined via EPMA-GMRFILM methodology.

A detailed technical paper on effects of interfacial carbide layer characteristics on thermal properties of copper-diamond composites was published online (V. Sinha, and J.E. Spowart, "Influence of Interfacial Carbide Layer Characteristics on Thermal Properties of Copper-Diamond Composites", Journal of Materials Science, 2012, doi: 10.1007/s10853-012-6878-0). In addition, a specimen with a different

interfacial Ti-layer thickness between Cu and diamond than previously characterized, was prepared for TDTR examination.

Previously, a natural diamond substrate had been used for the determination of Cu/diamond interface thermal conductance via TDTR. In the last year of the project, two synthetic single crystal diamond substrates (prepared via chemical vapor deposition, CVD) were acquired. Synthetic diamond substrates were characterized with electron backscattered diffraction (EBSD) technique to confirm that they indeed are single crystals. Magnetron sputtering experiments were carried out to deposit metal layers on diamond substrates: Cu was deposited on synthetic diamond, whereas Cu with a Ti interface layer was deposited on natural diamond. The sputtering parameters were selected to deposit a thicker interface layer of Ti than in previous experiments.

A final technical paper was drafted in May 2014, which summarized the technical effort for the entire project, including detailed results from TDTR experiments on both the natural diamond substrates and the synthetic single-crystal substrates prepared via CVD. Characterizations of the as-deposited copper and titanium layers of different thicknesses are compared, and related back to the underlying chemistries of the substrates. The full technical paper "Effects of Disorder State, Surface Roughness and Interfacial Layer on Thermal Transport in Copper/Diamond System" by V. Sinha, J.J. Gengler, C. Muratore and J.E. Spowart is included in Appendix A for completeness.

2.0   RESULTS

The GMR Film model of the data acquired in EPMA suggested that the thickness of interfacial chromium-carbide layer varies with the diamond content in Fraunhofer-supplied CuCr-diamond composites. For the diamond particles extracted from Cu-SiC-diamond composite, the GMR Film model of EPMA data did not provide self-consistent results. Several possible modifications of methodology were considered with an aim to obtain self-consistent and reliable results.

The thickness values of Ti and Cu layers deposited on the natural diamond substrates, as determined with EPMA – GMRFILM methodology, are: Ti layer = 2.3 nm and Cu layer = 133 nm. Using the TDTR experiment and modeling, the thermal conductance for Cu/diamond interface ($G_{Cu/diamond}$) in this specimen was determined to be 99 ± 7 MW m^{-2} K^{-1}. Earlier measurements of $G_{Cu/diamond}$ with TDTR indicated values of 34 and 58 MW m^{-2} K^{-1} for specimens with no interfacial Ti-layer and with 1.5 nm thick interfacial Ti-layer, respectively. Therefore, the thermal conductance across Cu/diamond interface appears to increase with an increase in interfacial Ti-layer thickness.

Good TDTR signals were received from the Cu-coated synthetic diamond substrates, suggesting the surface finish of these substrates is adequate for TDTR experiments. The values of thickness of metallic layers, as determined with EPMA-GMRFILM model were as follows: 248 nm Cu top layer and 3.7 nm Ti interface layer on natural diamond substrate, and 267 nm Cu on synthetic diamond substrate. Ti interface layer thickness was close to the target value of 4 nm. However, the Cu top layer was significantly thicker than the target value of 100 nm on both the substrates. Nevertheless, the TDTR data were modeled to determine the Cu/diamond interface thermal conductance ($G_{Cu/diamond}$) values. The $G_{Cu/diamond}$ was determined to be 133 ± 14 MW m^{-2} K^{-1} for the sample with natural diamond substrate, and it was 110 ± 10 MW m^{-2} K^{-1} for the sample with synthetic diamond substrate. This indicates a further improvement in $G_{Cu/diamond}$ for a still thicker Ti interface layer (as described in the previous report, $G_{Cu/diamond}$ was 34, 58 and 99 MW m^{-2} K^{-1} for samples with 0, 1.5 and 2.3 nm thick interface Ti layers, respectively). Moreover, the $G_{Cu/diamond}$ for the sample with synthetic diamond substrate was three times higher than for the sample with natural diamond substrate (no Ti interface layer in both cases). However, to model the TDTR data on the two most recent samples (i.e. natural diamond/3.7 nm Ti/248 nm Cu, and synthetic diamond/267 nm Cu), data corresponding to the pump advance of first 300-600 ps needed to be neglected. This could possibly be due to a significantly thicker Cu top layer than the target value of 100 nm, as data corresponding to the pump advance of first 100 ps usually need to be neglected in the modeling.

The EBSD patterns for the synthetic and natural diamond substrates at different locations throughout the top polished surface of each substrate remained essentially unchanged, which confirms that the substrates are single crystals. Several of the Kikuchi bands had to be detected manually. Since the procedure involving manual detection of bands provides more accurate crystallographic orientation than the automated detection, the manual band detection method was employed in the current study for characterization of diamond substrates, even though the automated method is faster. The manual detection method has been used previously to determine the crystallographic orientation of fracture facets in Ti-alloys.

SIMS depth profiles for the synthetic and natural diamond substrates showed that the surface nitrogen concentration in synthetic diamond is one order of magnitude lower than in natural diamond. The nitrogen concentration of natural diamond remains essentially unchanged with depth, whereas for synthetic diamond it decreases by three orders of magnitude in the first 0.6 μm and remains essentially unchanged at higher depths. The bulk nitrogen concentration of synthetic diamond substrate is 2.2×10^{16} atoms/cm^3 (*i.e.* 0.15 ppm by weight), which is approximately four orders of magnitude smaller than the value of 1.33×10^{20} atoms/cm^3 (*i.e.* 883 ppm by weight) for natural diamond substrate. The hydrogen, oxygen, sulfur, chlorine and fluorine concentrations also remain essentially unchanged with depth for natural diamond substrate, whereas for synthetic diamond these decrease by two to three orders of magnitude in the first

0.5 – 1.2 µm and remain essentially unchanged at higher depths. The bulk concentrations of H, O, S, Cl and F in both the diamond substrates are below the detection limit for the element of interest.

The surface profiles for the two substrates showed that the roughness of synthetic diamond is higher than the natural diamond. The root mean squared roughness (R_q) values for synthetic and natural diamonds are 5.8 and 2.8 nm, respectively. The average roughness (R_a) values for the same materials are 2.3 and 1.6 nm, respectively. Furthermore, the surface topography of natural diamond is more uniform than synthetic diamond. The thickness of the Ti-interface layer ranged between 0 and 3.5 nm on different specimens, as determined with GMRFILM modeling of data acquired in an EPMA. The thickness of Cu top layer was also determined with GMRFILM modeling of EPMA data, and it varied in the range 73-133 nm for different specimens.

The h_c values calculated through modeling of two-color TDTR data are depicted in Fig. 1 for the two types of diamond substrates (synthetic and natural) and for a range of thicknesses of Ti-interface layer. Each of the data points in Fig. 1 is an average of measurements at five different locations on a specimen, and the error bars indicate standard deviation for the five measurements on a particular specimen. Two specimens with the synthetic diamond substrate and without any Ti-interface layer were prepared, and characterized with TDTR. The h_c values for these two specimens are shown as two different data points in Fig. 1, and demonstrate that the reproducibility of methodology, including specimen preparation and TDTR characterization, employed in the current study is within ±10%.
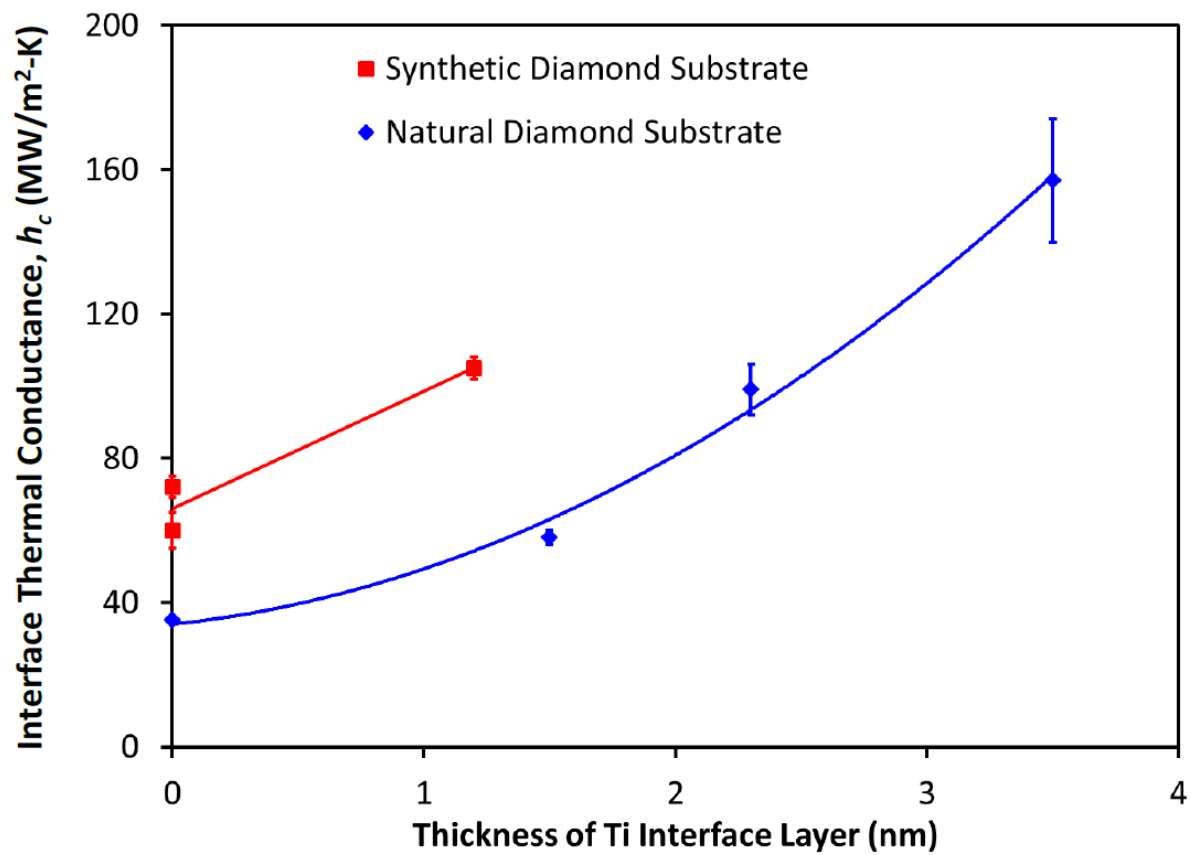
Figure 1: showing calculated h_c values from modeling of the experimental TDTR data for both the CVD (synthetic) and natural diamond substrates, with a range of thicknesses of the Ti interface layer.

3.0   CONCLUSIONS

The interface thermal conductance between Cu and diamond was measured using TDTR method. Very thin Ti interface layers ($\leq$ 3.5 nm thick) were introduced between Cu and diamond, and effects of presence of Ti at the interface as well as variation in its thickness on h_c were examined. The specimens for TDTR characterization were prepared via magnetron sputtering of metal layers (Cu and Ti) on synthetic and natural single crystal diamond substrates. The results indicate that the values of h_c for specimens with synthetic diamond substrate are ~ 2× higher than for specimens with natural diamond substrate. This difference can be attributed to: (a) lower level of disorder in near-surface region and a higher λ of synthetic diamond substrate, as a result of significantly lower nitrogen concentration, and/or (b) a higher surface roughness of synthetic diamond substrate. Furthermore, the presence of Ti-interface layer increases the h_c in specimens with both the synthetic and natural diamond substrates. The h_c is directly related to the Ti-interface layer thickness, within the range of thicknesses examined in the current study. A mechanism based on the expected variations of effective mean free path of electrons with Ti-interface layer thickness is suggested to explain this anomalous behavior.

Approved for public release; distribution unlimited.

APPENDIX A

Effects of Disorder State, Surface Roughness and Interfacial Layer on Thermal Transport in Copper/Diamond System

V. Sinha[1, 2], J.J. Gengler[1,3], C. Muratore[1,4], and J.E. Spowart[1]

[1]Air Force Research Laboratory, Materials and Manufacturing Directorate,

Wright-Patterson Air Force Base, OH 45433, USA

[2]UES, Inc., 4401 Dayton-Xenia Road, Dayton, OH 45432, USA

[3]Spectral Energies, LLC, 5100 Springfield Street, Suite 301, Dayton, Ohio 45431, USA

[4]University of Dayton Research Institute, 300 College Park, Dayton, Ohio 45469, USA

Abstract

Characterization of Cu/diamond interface thermal conductance (h_c) and an improved understanding of factors affecting it are important, as Cu-diamond composites are increasingly being considered for electronic packaging applications. In this study, ~90 nm thick Cu layer was deposited on synthetic as well as natural diamond substrates. In several specimens, a Ti-interface layer of thickness ≤ 3.5 nm was sputtered between the diamond substrate and the Cu top layer. The h_c across Cu/diamond interfaces for the specimens with and without a Ti-interface layer was determined with time-domain thermoreflectance. The h_c is ~ 2× higher for specimens with the synthetic diamond substrate than with natural diamond. The roughness of synthetic diamond substrate is ~ 2 × higher than natural diamond. The surface nitrogen concentration of synthetic diamond substrate is an order of magnitude lower than natural diamond and bulk nitrogen concentration is four orders of magnitude lower in synthetic diamond. These differences in roughness and nitrogen concentration can potentially explain the variations in h_c. Furthermore, the h_c was observed to increase with an increase of Ti-interface layer thickness. This is explained by invoking Fuchs-Sondheimer (size-effect) theory, which suggests that with an increase of Ti-interface layer thickness, the effective mean free path of electrons in Ti-layer increases with a concomitant increase in its thermal conductivity.

1. INTRODUCTION:

For reliable operation of high power density electronic devices, an efficient heat removal from hot regions is required. The thermal properties of Cu-diamond composites make them preferred materials for these heat sink applications, and this composite has been investigated extensively in recent years [1,2,3,4]. A maximization of metal/diamond interface thermal conductance (h_c) is a promising path to maximize the composite thermal conductivity (λ) [5,6]. Therefore, examinations of h_c for Cu/diamond interface and factors influencing it are both of scientific interest and practical importance.

In the absence of an interface layer between Cu and diamond, the h_c for Cu/diamond interfaces are quite low and this causes λ of composites also to be very low. For example, Schubert *et al.* [7] reported λ = 215 W/m-K for a Cu-42 vol% diamond composite with no interfacial layer. The λ of composite in this case is significantly lower than Cu (~400 W/m-K). Thus, the addition of diamond in Cu matrix, in this example, does not lead to any improvement in its ability to spread heat and in fact, deteriorates it. The h_c was calculated to be 0.5 MW/m²-K for this composite and this low value of h_c resulted in the low λ [8]. The introduction of an interfacial thin carbide (*e.g.* Cr_3C_2, B_4C, TiC, etc.) layer between Cu and diamond is known to increase the λ of Cu-diamond composites to values well above the λ of Cu, which is effected due to the improvement in h_c [9,10,11,12,13,14]. It is also established that h_c is inversely related to the thickness of the interfacial carbide layer [15]. The calculation of h_c in prior studies [16,17,18,19,20] invoked Hasselman-Johnson [21] and/or differential effective medium [22] models, which require the composite λ to be one of the input parameters.

There is an alternate method, time-domain thermoreflectance (TDTR) [23,24,25,26,27], to determine h_c for metal/diamond interfaces, which allows precise and more direct measurement for an individual interface rather than an average over a bulk sample. The sample for TDTR examination can be prepared by deposition of thin metallic layers (~ 90 nm thick) on a diamond substrate. The metal layers are locally heated (temperature increase is ≤ 1 K) with a pump laser beam, and the change in its reflectance with time and temperature is monitored with a probe laser beam. The modeling of changes in reflectance of metal top layers leads to the determination of h_c. Several studies employed TDTR or similar techniques to determine h_c for metal/diamond interfaces [28,29,30]. Recent advances with two-color [31,32,33] TDTR have greatly improved the characterization of specimens with a Cu top layer. Gengler *et al.* [34] reported an h_c ~ 60 MW/m²-K for an interface between Cu and highly oriented pyrolitic graphite (HOPG), whereas Monachon and Weber [35] reported an h_c ~ 35 MW/m²-K for an interface between Cu and diamond. There are no prior reports on TDTR-determined h_c of a material system, where an interface layer is introduced between Cu and diamond.

In the current research, a Ti interface layer is introduced between Cu and diamond, and the h_c for this material system is determined with TDTR. The objective of this study is to determine if the presence of a Ti interface layer improves the h_c, akin to an enhancement effected by carbide interface layers in the case of Cu-diamond composites. Furthermore, the thickness of Ti interface layer is systematically varied and the h_c is determined using TDTR for different Ti layer thicknesses. This part of study was aimed at identifying any correlations between h_c and the Ti interface layer thickness. Stoner and Maris [36] have used molecular-dynamics simulations to demonstrate that the strength of the potential binding metal to

the substrate has a significant effect on the predicted h_c, with a higher strength resulting in a higher h_c. Transition metals such as Ti and Cr bond strongly to carbon and moreover, Ti has a stronger bond with carbon than Cr [37]. Therefore, Ti is selected to be the interface layer between Cu and diamond in the current study.

In their seminal paper [38], Swartz and Pohl concluded that bulk disorder near the interface can cause significant deviations in the experimentally determined h_c from its model prediction. In the current study, the concentrations of nitrogen and other impurities (*e.g.* hydrogen, oxygen, etc.) were measured as these may contribute to the disorder. Secondary ion mass spectrometry (SIMS) was used for concentration measurements as a function of depth below the sample surface. Atomic force microscopy (AFM) was used to measure the surface roughness of diamond substrates. The differences in h_c of specimens with synthetic and natural diamond substrates are discussed in the context of variations in near-surface disorder and interfacial roughness.

2. EXPERIMENTAL PROCEDURES:

In this study two different types of single crystal diamond substrates, synthetic and natural, were used to make specimens for h_c determinations. The synthetic and natural diamond substrates were supplied by Element Six (Santa Clara, CA) and Blue Nile (Seattle, WA), respectively. The crystallographic orientation was determined with electron backscattered diffraction (EBSD) techniques in a scanning electron microscope (SEM). An FEI XL-30 SEM with a field emission gun (FEG) as the electron source was used. The diamond substrates were tilted at 70° in the SEM sample chamber, and the EBSD patterns were acquired with TSL (Draper, UT, USA) OIM Data Collection software at an accelerating voltage of 20 kV and a working distance of 25 mm. Several Kikuchi bands in each EBSD pattern were detected manually and indexing of pattern yields the crystallographic orientation of diamond substrates. The EBSD technique of crystallographic orientation determination is known to be accurate within $\pm 1^\circ$ [39]. The crystallographic orientations of diamond substrates were depicted in inverse pole figures using TSL OIM Analysis software.

The SIMS experiments were carried out in a Cameca unit with Cs^+ as the primary ion beam at 14.5 keV. The concentrations of six elements (nitrogen, hydrogen, oxygen, fluorine, chlorine and sulfur) as a function of depth were measured in both the synthetic and natural diamond substrates. CN^-, H^-, O^-, F^-, Cl^- and S^- secondary ions were monitored for concentration quantification of N, H, O, F, Cl and S, respectively. To minimize the contributions of $^{13}C_2^-$ to CN^- counts, high mass resolution spectrum was utilized in the case of CN^- secondary ions. The conversion of the measured secondary ion counts to concentration was accomplished using relative sensitivity factors from carbon standards. The depth scale was calibrated by measuring the depth of analysis crater with a stylus profilometer. The detection limits for the different elements are shown in Table 1.

Table 1: Detection Limits of Analyzed Elements in Diamond

Element	Detection Limit (atoms/cm^3)
H	2×10^{17}
N	2×10^{15}
O	5×10^{16}
F	5×10^{14}
S	1×10^{15}
Cl	1×10^{15}

The roughness was measured *via* AFM in a Bruker Nanoscope. The scan size was 30 μm × 30 μm, the scan rate was 1 Hz and the measurements were conducted in the tapping mode.

The metal films were deposited on the diamond substrates via magnetron sputtering. A direct current (DC) process was used for deposition of Cu top layer; whereas high power pulsed magnetron sputtering process was used for deposition of Ti-interface layer. This process differs from ordinary sputtering in that 1) the metal flux is composed primarily of ions rather than neutrals, and 2) the maximum kinetic energy of the incident ions is significantly larger (~10-15 eV) than in ordinary sputtering. The base pressure for magnetron sputtering apparatus was less than 5×10^{-9} Torr, and the pure metal (Ti and Cu) targets were sputtered in 10 mTorr of ultra-high purity Ar. The maximum temperature of the substrate surface during deposition was approximately 70 °C as measured by a calibrated infrared pyrometer aimed at the sample surface.

The sputter-coated diamond substrates were characterized with electron probe microanalysis (EPMA) to determine the thickness of metallic thin film(s). The EPMA experiments were conducted using Cameca SX100 unit operating at 15 kV and/or 25 kV. Data from EPMA experiments were modeled to determine the metal layer thickness. Several software packages (*e.g.* GMRFILM, Strata and Multifilm) have been developed by different research groups to process the data acquired in an EPMA for determinations of film thickness and composition [40,41,42]. GMRFILM permits the determination of film thickness (with an accuracy of ±10%) from experimentally determined X-ray intensity ratios (*k*-ratios) and known film density, as described in ref. [43]. In the current work, the *k*-ratios for the elements of interest (*i.e.* Cu and Ti) were determined with EPMA experiments using wavelength-dispersive spectrometer (WDS) on the surface Cu-film on diamond substrates and on pure elemental (Cu and Ti) standards. The *k*-ratios and density of metals (ρ_{Cu} = 8.89×10^3 kg/m^3 and ρ_{Ti} = 4.51×10^3 kg/m^3) were entered in the GMRFILM program to calculate the metallic layer thicknesses. Similar results were obtained at EPMA accelerating voltages of 15 and 25 kV. Prior studies report a good correlation of thin film thickness values determined using EPMA with those determined using Transmission Electron Microscopy [44], Spectroscopic Ellipsometry [45] and Rutherford Backscattering Spectrometry [46,47] based techniques. The experiments in our laboratory on sputter-coated metal films also confirmed a good correlation of thin film thickness

values determined using EPMA - GMRFILM method with those determined using TEM, Profilometry and Rutherford Backscattering Spectrometry. Therefore, EPMA - GMRFILM technique is expected to provide accurate values of metallic layer thicknesses in the current research.

Thermal conductance of the Cu/diamond interfaces was determined with a two-color TDTR lab [48]. The output of a mode-locked Ti:sapphire laser is split into a pump and a probe beam. The pump beam (wavelength ~785 nm) is sent first through a pulse compressor and then through an electro-optic modulator (EOM), which imposes a square-wave pulse train with a frequency of 9.8 MHz. The pump beam is then aligned along a mechanical translation stage to systematically alter the timing between the pump and the probe pulses. The probe beam is sent through an optical parametric oscillator (OPO) to modify its wavelength to ~ 600 nm. Both beams are then focused to a spot size of ~50 μm at a 45° angle to the sample. The reflected probe beam is spatially filtered, recollimated, and sent through a 750 nm short pass optical filter to reject scattered pump-beam light. Finally, the probe beam is passed through a neutral-density filter (optical density = 1.0) and focused onto a silicon photodiode detector. The output of the detector is sent to the input of a dual phase, radio frequency lock-in amplifier that has its reference channel connected to the same electronic signal that drives the EOM. The scans and data acquisition are computer controlled with a LABVIEW program developed in our laboratory. TDTR data were acquired from five randomly chosen locations on each sample surface. Data analysis was performed with a nonlinear least squares application to Cahill's frequency domain model [49] to determine h_c for Cu/diamond interfaces. The results from the five scans of each sample were used to establish an average ± standard deviation value.

3. RESULTS:

The EBSD patterns for the synthetic and natural diamond substrates are shown in Fig. 1(a) and 1(d), respectively. The patterns at different locations throughout the top polished surface of each substrate remained essentially unchanged, which confirms that the substrates are single crystals. Several of the Kikuchi bands are detected manually and are shown as red lines in Fig. 1(b). The indexed patterns for synthetic and natural diamond substrates are shown in Fig. 1(c) and 1(e), respectively. Since the procedure involving manual detection of bands provides more accurate crystallographic orientation than the automated detection, the manual band detection method was employed in the current study for characterization of diamond substrates, even though the automated method is faster. The manual detection method has been used previously to determine the crystallographic orientation of fracture facets in Ti-alloys [50,51]. The crystallographic orientations of diamond substrates are shown in Fig. 2.
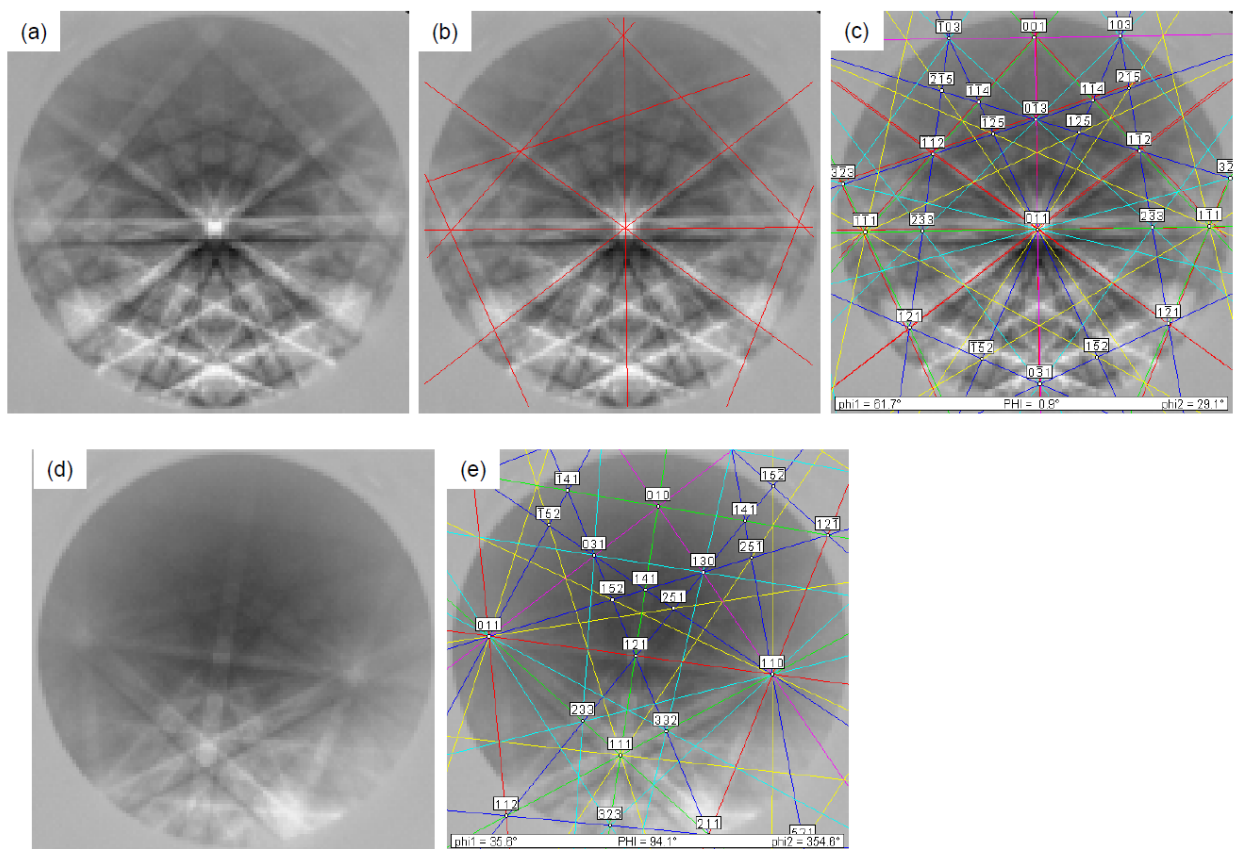
Figure 1: Determination of crystallography orientation of diamond substrates with electron backscattered diffraction (EBSD) technique in an SEM. (a) EBSD pattern from synthetic (CVD) diamond, (b) manual detection of Kikuchi bands in pattern (a), (c) indexing of pattern (a), (d) EBSD pattern from natural diamond, and (e) indexing of pattern (d).
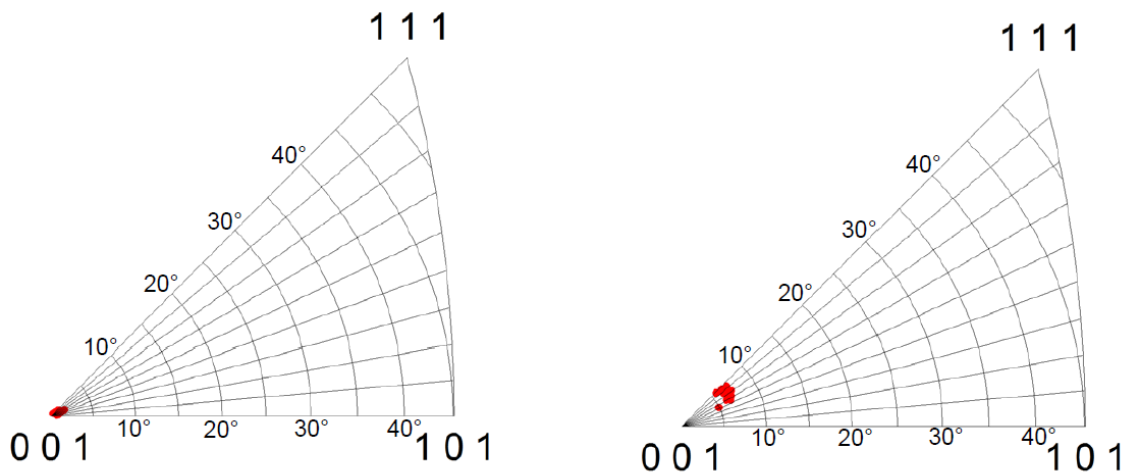

Figure 2: Inverse pole figures showing the crystallographic orientation of diamond substrates. The red closed circles depict the orientation of surface normal in the stereographic triangle for diamond crystal, which were determined with EBSD at 13 different locations on the substrate. (a) Synthetic diamond, and (b) natural diamond.

12

The SIMS depth profiles for the synthetic and natural diamond substrates are shown in Fig. 3 and 4. The surface nitrogen concentration in synthetic diamond is one order of magnitude lower than in natural diamond. The nitrogen concentration of natural diamond remains essentially unchanged with depth, whereas for synthetic diamond it decreases by three orders of magnitude in the first 0.6 μm and remains essentially unchanged at higher depths (Fig. 3). The bulk nitrogen concentration of synthetic diamond substrate is 2.2×10^{16} atoms/cm^3 (*i.e.* 0.15 ppm by weight), which is approximately four orders of magnitude smaller than the value of 1.33×10^{20} atoms/cm^3 (*i.e.* 883 ppm by weight) for natural diamond substrate. The hydrogen, oxygen, sulfur, chlorine and fluorine concentrations also remain essentially unchanged with depth for natural diamond substrate, whereas for synthetic diamond these decrease by two to three orders of magnitude in the first 0.5 – 1.2 μm and remain essentially unchanged at higher depths (Fig. 4). The bulk concentrations of H, O, S, Cl and F in both the diamond substrates are below the detection limit for the element of interest (Fig. 4 and Table 1).
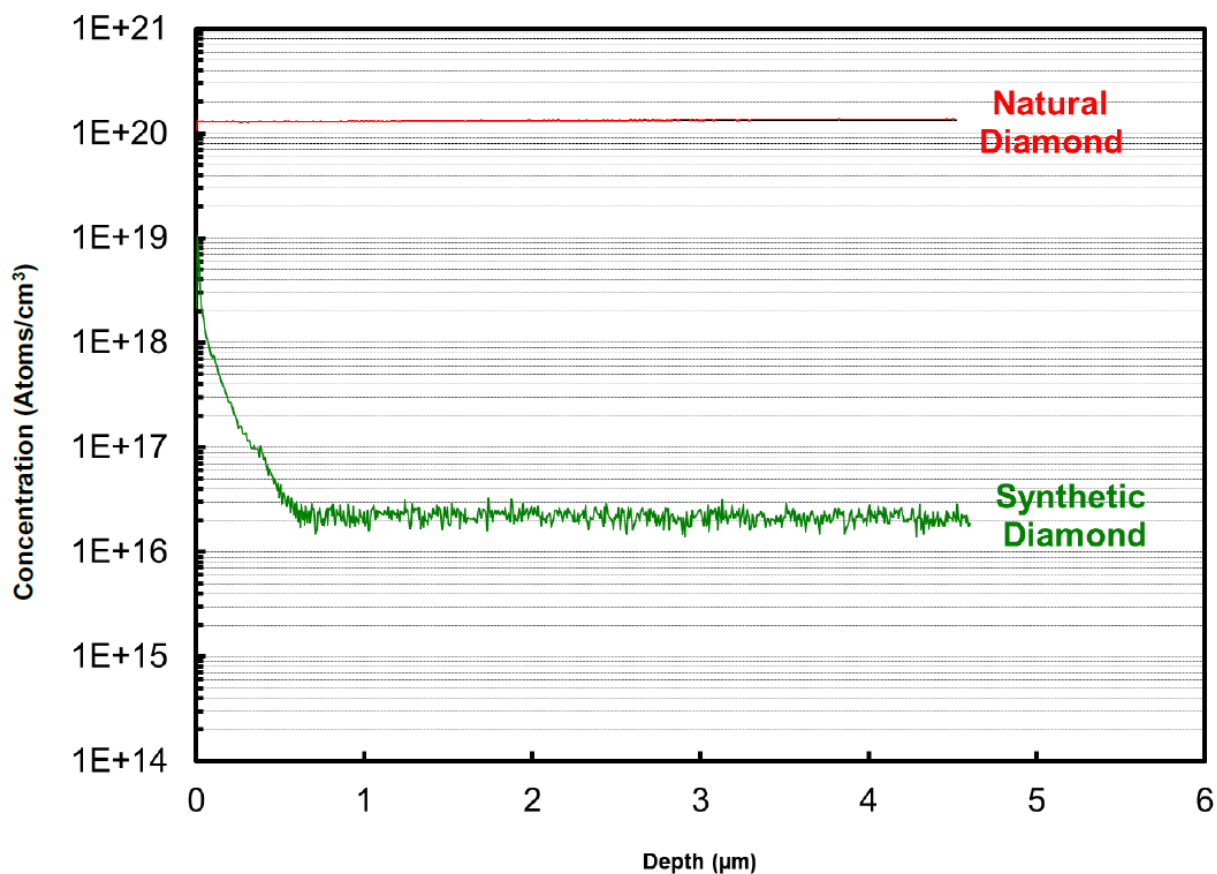

Figure 3: SIMS depth profiles showing nitrogen concentration as a function of depth below the surface for synthetic and natural diamond substrates.
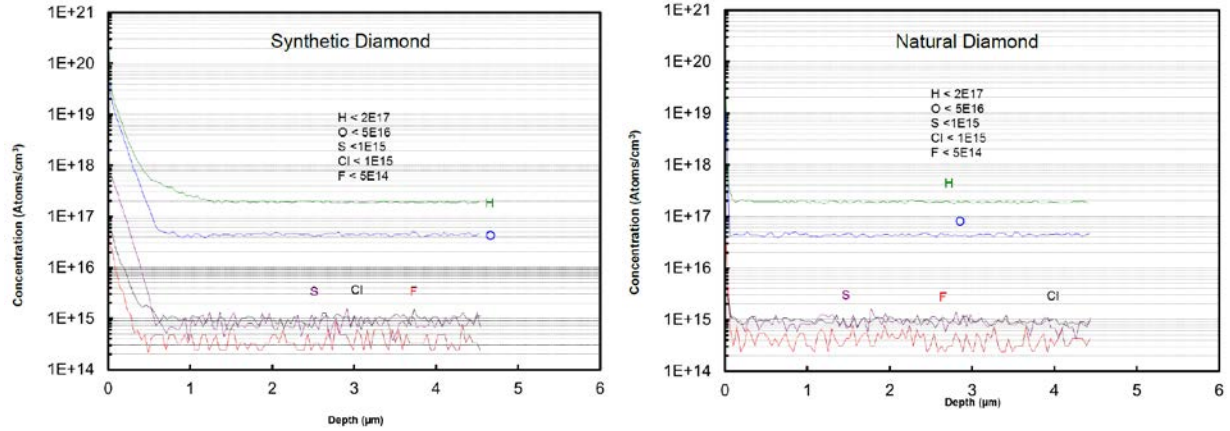
Figure 4: SIMS depth profiles showing concentrations of hydrogen, oxygen, sulfur, chlorine and fluorine as a function of depth below the surface for (a) synthetic, and (b) natural diamond substrates.

The surface profiles for the two substrates are shown in Fig. 5. The roughness of synthetic diamond is higher than the natural diamond. The root mean squared roughness (R_q) values for synthetic and natural diamonds are 5.8 and 2.8 nm, respectively. The average roughness (R_a) values for synthetic and natural diamonds are 2.3 and 1.6 nm, respectively. Furthermore, the surface topography of natural diamond is more uniform than synthetic diamond (Fig. 5).

The thickness of Ti-interface layer ranged between 0 and 3.5 nm on different specimens, as determined with GMRFILM modeling of data acquired in an EPMA. The thickness of Cu top layer was also determined with GMRFILM modeling of EPMA data, and it varied in the range 73-133 nm for different specimens.

The h_c values calculated through modeling of TDTR data are depicted in Fig. 6 for the two types of diamond substrates (synthetic and natural) and for a range of thicknesses of Ti-interface layer. Each of the data points in Fig. 6 is an average of measurements at five different locations on a specimen, and the error bars indicate standard deviation for the five measurements on a particular specimen. Two specimens with the synthetic diamond substrate and without any Ti-interface layer were prepared, and characterized with TDTR. The h_c values for these two specimens are shown as two different data points in Fig. 6, and demonstrate that the reproducibility of methodology, including specimen preparation and TDTR characterization, employed in the current study is within ±10%.

The acoustic mismatch model (AMM) [52] predicts a value of 48 MW/m²-K for the h_c across Cu/diamond interfaces [53,54,55]. The values of h_c determined with TDTR in the current study for specimens with no interfacial Ti are similar to the AMM prediction.
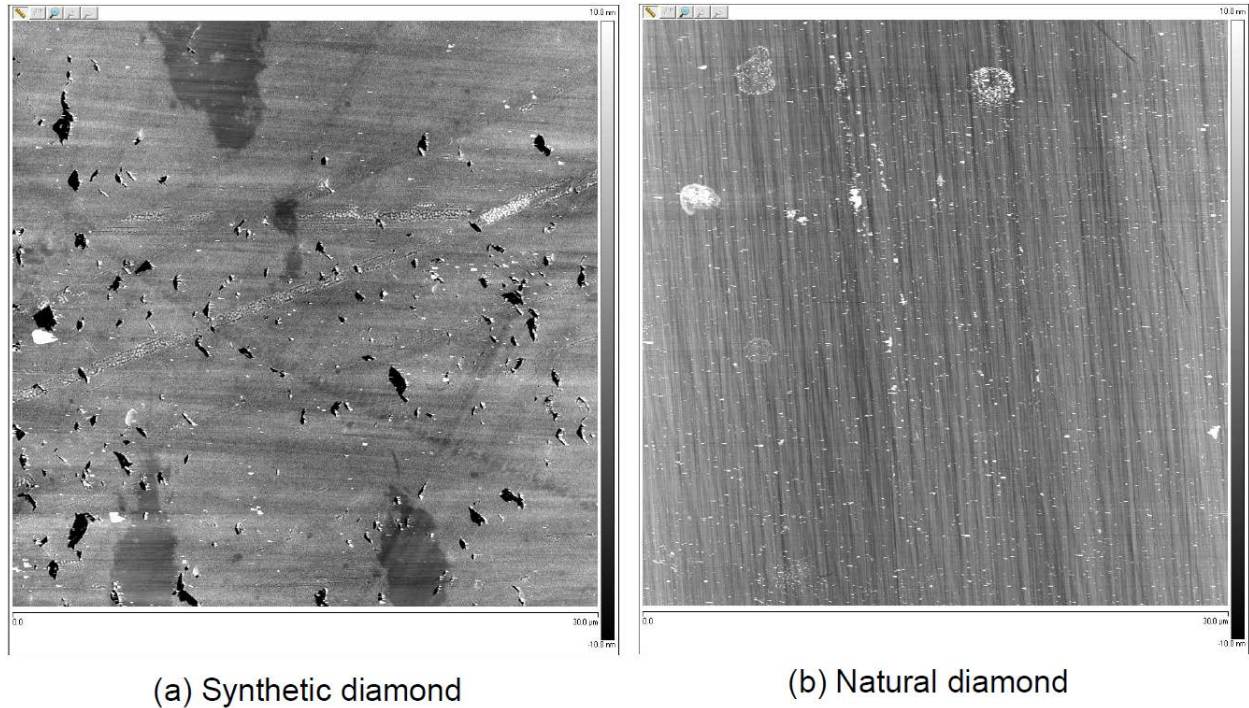
(a) Synthetic diamond   (b) Natural diamond

Figure 5: Surface profiles acquired with AFM. (a) Synthetic, and (b) natural diamond substrates.

4. DISCUSSION:

The h_c of specimens with synthetic diamond substrate is higher than with natural diamond substrate (Fig. 6). It is clear from Fig. 2 that the surface of both the diamond substrates is parallel to the (001) crystallographic plane. Thus, the crystallography of surface is essentially the same for two types of diamond substrates. The substantially lower nitrogen concentration in synthetic diamond than in natural diamond (Fig. 3) and essentially similar bulk concentrations of H, O, S, Cl and F in the two diamonds (Fig. 4) suggest that the degree of disorder in synthetic diamond is significantly less than in the natural diamond substrate. Since λ of diamond is known to decrease with an increase of its nitrogen content [56], this also implies that synthetic diamond has a higher λ. This is further supported by the modeling of TDTR data, which suggests that λ of synthetic diamond is higher than natural diamond. In this context, it is interesting to note that Swartz and Pohl have suggested that bulk disorder in the near-surface region can potentially cause significant variations in h_c and therefore, an understanding of this disorder is highly desirable [57]. The current study provides the experimental evidence of variations in nitrogen concentration of the natural and synthetic diamond substrates, which potentially can lead to variations in the degree of bulk disorder in near-surface regions of the two substrates. This can explain, at least in part, the differences in h_c of specimens with natural and synthetic diamond substrates. In addition to the differences in nitrogen concentration, the roughness and uniformity of surface topography for the two substrates are different. These differences can potentially lead to the variations in adherence of sputtered Cu film on the two diamond substrates and/or the electron-phonon coupling at the

15

Cu/diamond interface. These variations can also contribute to the observed differences in h_c of specimens with natural and synthetic diamond substrates.
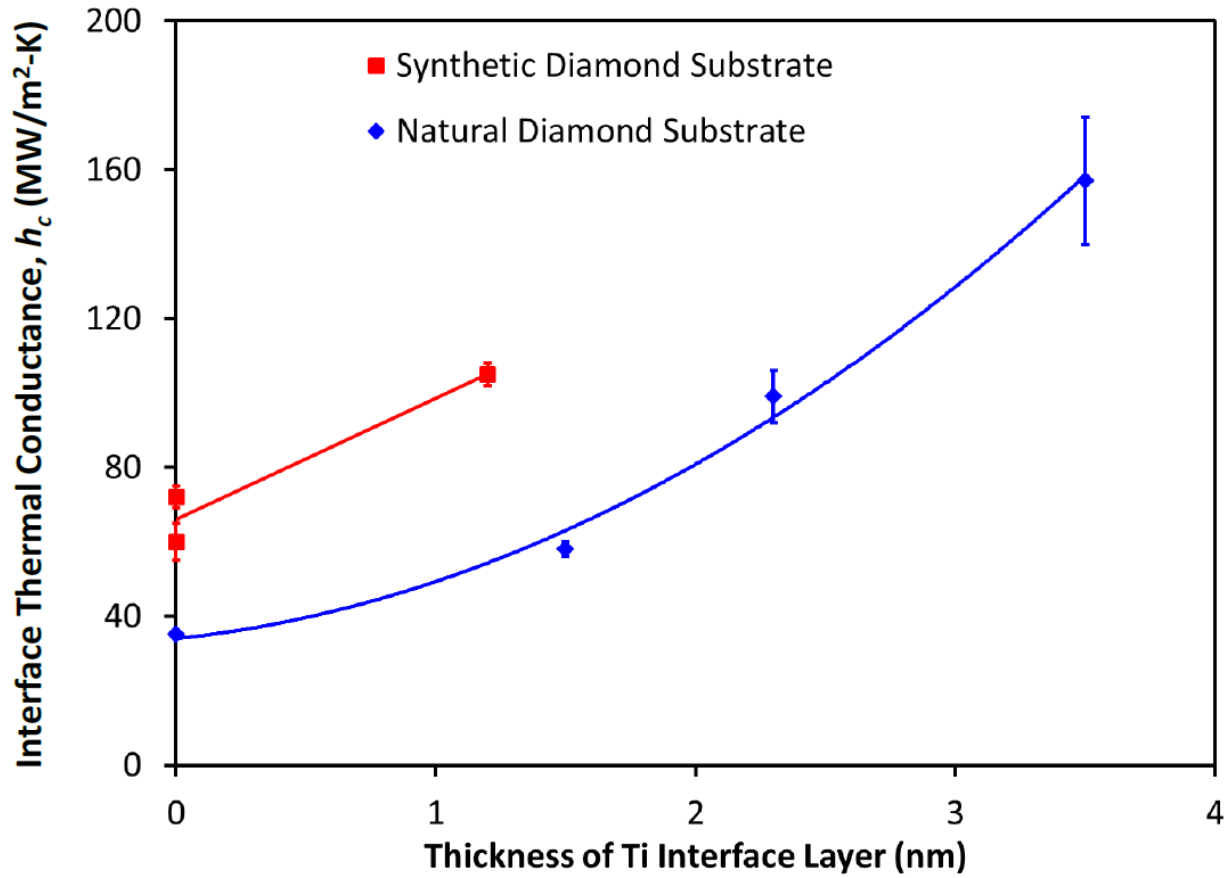

Figure 6: Effect of Ti Interface Layer Thickness on Cu/Diamond Interface Conductance. The h_c values were determined with a two-color TDTR set-up.

For specimens with both the synthetic and natural diamond substrates, the presence of Ti-interface layer causes an increase in h_c (Fig. 6). This is presumably due to a higher interfacial bond strength between Ti and diamond than between Cu and diamond. Both the simulations by Stoner and Maris [58] and the experimental work of Collins, *et al.* [59] suggest that the strength of interfacial bonding may have a strong influence on h_c, which can help rationalize the findings of current research.

For the specimens with natural diamond substrate, an increase in Ti-interface layer thickness results in an increase in h_c (Fig. 6). This can be understood in terms of Fuchs-Sondheimer size-effect theory [60,61] by considering the relative values of bulk mean free path (MFP) of heat carriers (*i.e.* electrons) in Ti and the Ti-interface layer thickness in TDTR specimens in the current study. The bulk MFP of conduction electrons in Ti at room temperature is 28.5 nm [62], which is at least 8× higher than the Ti-interface layer thicknesses examined in current study. In addition to the scattering mechanisms operational in bulk Ti, the electrons in interfacial Ti-layer in TDTR specimens of current study are also expected to scatter at Cu/Ti and Ti/diamond interfaces, which results in the effective MFP of electrons in Ti-interface layer to

16

be significantly less than the value of 28.5 nm for bulk Ti. For this case of Ti-interface layer thickness < MFP of electrons in bulk Ti, an increase of Ti-layer thickness is likely to increase the effective MFP of electrons, which in turn is expected to cause an increase in λ of interfacial Ti-layer [63] and thereby, an increase in effective h_c across Cu/diamond interfaces in the specimens examined in current study. In one set of Cu-diamond composites examined by Abyzov, *et al.* [64], the λ of composite increased with an *increase* of tungsten interface layer thickness, which is consistent with the results of current study.

Schmidt, *et al.* [65] reported that the values of h_c for a Ti/c-oriented HOPG specimen and an Al/c-oriented HOPG specimen with a 5 nm thick Ti-adhesion (interface) layer between Al and HOPG were similar. By analogy, it is expected that the h_c for a Cu/diamond specimen with a 3.5 nm thick Ti-interface layer in the current study will be similar to a Ti/diamond specimen. Stoner and Maris [66] measured an h_c = 100 MW/m²-K for Ti/diamond specimen at room temperature, which is lower than 157 MW/m²-K measured in the current study for a Cu/diamond specimen with 3.5 nm thick Ti-interface layer. This difference could be associated with possible differences in the nitrogen concentration and/or surface roughness of the diamond substrates in the two studies, as was observed for the specimens with the synthetic and natural diamond substrates in the current study. Furthermore, the lattice dynamical calculations predict a value of 70 MW/m²-K for h_c across Ti/diamond interface [67], which again is lower than the h_c of 157 MW/m²-K for the Cu/diamond specimen with a 3.5 nm thick Ti-interface layer characterized in the current study. However, the diffuse mismatch limit is higher than the prediction of lattice dynamics modeling, and radiation limit is even higher than the diffuse mismatch limit [68]. It is expected that the diffuse mismatch and radiation limits for Ti/diamond interface will better match the h_c measured in current study for Cu/diamond specimen with a 3.5 nm thick Ti-interface layer.

5. SUMMARY AND CONCLUSIONS:

The interface thermal conductance between Cu and diamond was measured using TDTR method. Very thin Ti interface layers (≤ 3.5 nm thick) were introduced between Cu and diamond, and effects of presence of Ti at the interface as well as variation in its thickness on h_c were examined. The specimens for TDTR characterization were prepared via magnetron sputtering of metal layers (Cu and Ti) on synthetic and natural single crystal diamond substrates. The results indicate that the values of h_c for specimens with synthetic diamond substrate are ~ 2× higher than for specimens with natural diamond substrate. This difference can be attributed to: (a) lower level of disorder in near-surface region and a higher λ of synthetic diamond substrate, as a result of significantly lower nitrogen concentration, and/or (b) a higher surface roughness of synthetic diamond substrate. Furthermore, the presence of Ti-interface layer increases the h_c in specimens with both the synthetic and natural diamond substrates. The h_c is directly related to the Ti-interface layer thickness, within the range of thicknesses examined in the current study. A mechanism based on the expected variations of effective mean free path of electrons with Ti-interface layer thickness is suggested to explain this anomalous behavior.

References

[1] Zweben C (2004) In: Zediker MS (ed) High-Power Diode Laser Technology and Applications II, Proc SPIE Vol. 5336, Bellingham, WA, pp. 166-175.

[2] Weber L, Tavangar R (2007) Scr Mater 57:988-991.

[3] V. Sinha, and J.E. Spowart, Journal of Materials Science, vol. 48, Issue 3, pp. 1330-1341, 2013 (doi: 10.1007/s10853-012-6878-0).

[4] Schubert T, Trindade B, Weißgärber T, Kieback B (2008) Mater Sci Eng A 475:39-44.

[5] V. Sinha, and J.E. Spowart, Journal of Materials Science, vol. 48, Issue 3, pp. 1330-1341, 2013 (doi: 10.1007/s10853-012-6878-0).

[6] R. Tavangar, and L. Weber, Emerging Materials Research, Volume 1, Issue EMR2, Pages 67–74, 2012 (doi: 10.1680/emr.11.00020).

[7] Schubert T, Trindade B, Weißgärber T, Kieback B (2008) Mater Sci Eng A 475:39-44.

[8] Schubert T, Trindade B, Weißgärber T, Kieback B (2008) Mater Sci Eng A 475:39-44.

[9] V. Sinha, and J.E. Spowart, Journal of Materials Science, vol. 48, Issue 3, pp. 1330-1341, 2013 (doi: 10.1007/s10853-012-6878-0).

[10] Schubert T, Trindade B, Weißgärber T, Kieback B (2008) Mater Sci Eng A 475:39-44.

[11] Schubert T, Ciupiński Ł, Zieliński W, Michalski A, Weißgärber T, Kieback B (2008) Scr Mater 58:263-266.

[12] Weber L, Tavangar R (2007) Scr Mater 57:988-991.

[13] Y. Zhang, H.L. Zhang, J.H. Wu and X.T. Wang, Scripta Materialia 65 (2011) 1097–1100.

[14] Ł. Ciupiński, D. Siemiaszko, M. Rosiński, A. Michalski and K.J. Kurzydłowski, Advanced Materials Research Vol. 59 (2009) pp 120-124.

[15] V. Sinha, and J.E. Spowart, Journal of Materials Science, vol. 48, Issue 3, pp. 1330-1341, 2013 (doi: 10.1007/s10853-012-6878-0).

[16] V. Sinha, and J.E. Spowart, Journal of Materials Science, vol. 48, Issue 3, pp. 1330-1341, 2013 (doi: 10.1007/s10853-012-6878-0).

[17] Schubert T, Trindade B, Weißgärber T, Kieback B (2008) Mater Sci Eng A 475:39-44.

[18] Schubert T, Ciupiński Ł, Zieliński W, Michalski A, Weißgärber T, Kieback B (2008) Scr Mater 58:263-266.

[19] Tavangar R, Molina JM, Weber L (2007) Scr Mater 56:357-360.

[20] Y. Zhang, H.L. Zhang, J.H. Wu and X.T. Wang, Scripta Materialia 65 (2011) 1097–1100.

Approved for public release; distribution unlimited.

[21] Hasselman DPH, Johnson LF (1987) J Compos Mater 21(6):508-15.

[22] Tavangar R, Molina JM, Weber L (2007) Scr Mater 56:357-360.

[23] H.-K. Lyeo and D.G. Cahill, Physical Review B 73, 144301 (2006).

[24] J.J. Gengler, C. Muratore, A.K. Roy, J. Hu, A.A. Voevodin, S. Roy, and J.R. Gord, Composites Science and Technology 70 (2010) 2117–2122.

[25] J.J. Gengler, S. Roy, J.G. Jones, and J.R. Gord, Meas. Sci. Technol. 23, 055205 (2012).

[26] D.G. Cahill, Rev Sci Instrum 75:5119–22 (2004).

[27] B.C. Gundrum, D.G. Cahill, and R.S. Averback, Physical Review B 72, 245426 (2005).

[28] R.J. Stoner and H.J. Maris, Phys. Rev. B 48, pp. 16373-16387, 1993.

[29] K.C. Collins, S. Chen, and G. Chen, Applied Physics Letters 97, 083102 (2010).

[30] C. Monachon and L. Weber, Emerging Materials Research, Volume 1, Issue EMR2, Pages 89–98, 2012 (doi: 10.1680/emr.11.00011).

[31] J.J. Gengler, S.V. Shenogin, J.E. Bultman,A.K. Roy, A.A. Voevodin, and C. Muratore, Journal of Applied Physics 112, 094904 (2012).

[32] J.J. Gengler, S. Roy, J.G. Jones, and J.R. Gord, Meas. Sci. Technol. 23, 055205 (2012).

[33] C. Monachon and L. Weber, Emerging Materials Research, Volume 1, Issue EMR2, Pages 89–98, 2012 (doi: 10.1680/emr.11.00011).

[34] J.J. Gengler, S.V. Shenogin, J.E. Bultman,A.K. Roy, A.A. Voevodin, and C. Muratore, Journal of Applied Physics 112, 094904 (2012).

[35] C. Monachon and L. Weber, Emerging Materials Research, Volume 1, Issue EMR2, Pages 89–98, 2012 (doi: 10.1680/emr.11.00011).

[36] R.J. Stoner and H.J. Maris, Phys. Rev. B 48, pp. 16373-16387, 1993.

[37] A.J. Schmidt, K.C. Collins, A. Minnich and G. Chen, Journal of Applied Physics 107, 104907 (2010).

[38] Swartz ET, Pohl RO (1989) Rev Mod Phys 61(3):605-668.

[39] M.C. Demirel, B.S. El-Dasher, B.L. Adams, and A.D. Rollett (2000) In: Schwartz AJ, Kumar M, Adams BL (eds) Electron backscatter diffraction in materials science. Kluwer Academic/Plenum Publishers, New York, NY, pp 65-74.

[40] Waldo RA, Militello MC, Gaarenstroom SW (1993) Surf Interface Anal 20:111-114

20

[41] Pouchou JL, Pichoir F (1993) Scanning Microsc Suppl 7:167-189

[42] Pouchou JL (1993) Anal Chim Acta 283:81-97

[43] Waldo RA, Militello MC, Gaarenstroom SW (1993) Surf Interface Anal 20:111-114

[44] Waldo RA, Militello MC, Gaarenstroom SW (1993) Surf Interface Anal 20:111-114

[45] Waldo RA, Militello MC, Gaarenstroom SW (1993) Surf Interface Anal 20:111-114

[46] Waldo RA, Militello MC, Gaarenstroom SW (1993) Surf Interface Anal 20:111-114

[47] Pouchou JL (1993) Anal Chim Acta 283:81-97

[48] J. J. Gengler, S. Roy, J. G. Jones, and J. R. Gord, Meas. Sci. Technol. 23, 055205 (2012).

[49] D. G. Cahill, Rev. Sci. Instrum. 75, 5119 (2004).

[50] V. Sinha, M.J. Mills, and J.C. Williams, Journal of Materials Science, vol. 42, no. 19, pp. 8334-8341, 2007.

[51] V. Sinha, M.J. Mills, and J.C. Williams, Metallurgical and Materials Transactions A, vol. 37A, pp. 2015-2026, 2006.

[52] Swartz ET, Pohl RO (1989) Rev Mod Phys 61(3):605-668.

[53] Chu K, Liu Z, Jia C, Chen H, Liang X, Gao W, Tian W, Guo H (2010) J Alloy Compd 490:453-458.

[54] Chu K, Jia C, Liang X, Chen H, Gao W, Guo H (2009) Mater Des 30:4311-4316.

[55] V. Sinha, and J.E. Spowart, Journal of Materials Science, vol. 48, Issue 3, pp. 1330-1341, 2013 (doi: 10.1007/s10853-012-6878-0).

[56] Yamamoto Y, Imai Y, Tanabe K, Tsuno T, Kumazawa Y, Fujimori N (1997) Diam Relat Mater 6:1057-1061.

[57] Swartz ET, Pohl RO (1989) Rev Mod Phys 61(3):605-668.

[58] R.J. Stoner and H.J. Maris, Phys. Rev. B 48, pp. 16373-16387, 1993.

[59] K.C. Collins, S. Chen, and G. Chen, Applied Physics Letters 97, 083102 (2010).

[60] K. Fuchs, Proc. Camb. Phil. Soc., 34 (1937-38) 100.

[61] E. H. Sondheimer, Advan. Phys., 1 (1952) 1.

[62] B. Singh and N. A. Surplice, Thin Solid Films, 10 (1972) 243-253.

Approved for public release; distribution unlimited.

[63] J.S. Jin, J.S. Lee, and O. Kwon, Applied Physics Letters 92, 171910 (2008).

[64] A.M. Abyzov, S.V. Kidalov, and F.M. Shakhov, J Mater Sci (2011) 46:1424–1438.

[65] A.J. Schmidt, K.C. Collins, A. Minnich and G. Chen, Journal of Applied Physics 107, 104907 (2010).

[66] R.J. Stoner and H.J. Maris, Phys. Rev. B 48, pp. 16373-16387, 1993.

[67] R.J. Stoner and H.J. Maris, Phys. Rev. B 48, pp. 16373-16387, 1993.

[68] R.J. Stoner and H.J. Maris, Phys. Rev. B 48, pp. 16373-16387, 1993.

LIST OF ACRONYMS, ABBREVIATIONS AND SYMBOLS

CVD   Chemical Vapor Deposition

DEM   Differential Effective Medium

EBSD   Electron Back-Scatter Diffraction

EPMA   Electron Probe Micro Analysis

G   Thermal conductance (units: $W\ m^{-2}\ K^{-1}$)

GMR   General Motors Research

SIMS   Secondary Ion Mass Spectrometry

TDTR   Time-Domain Thermo Reflectance